Improving Accuracy of Mobile Robot Localization by Tightly Fusing LiDAR and DR data

Yuan Xu[1(✉)], Yuriy S. Shmaliy[2], Tao Shen[1], Shuhui Bi[1], and Hang Guo[3]

[1] School of Electrical Engineering, University of Jinan, Jinan 250022, China
xy_abric@126.com, {cse_st,cse_bish}@ujn.edu.cn
[2] Department of Electronics Engineering, Universidad de Guanajuato, 36885 Salamanca, Mexico
shmaliy@ugto.mx
[3] Institute of Space Science and Technology, Nanchang University, Nanchang 330031, China
hguo@ncu.edu.cn

Abstract. In this paper, a tightly-coupled light detection and ranging (LiDAR)/dead reckoning (DR) navigation system with uncertain sampling time is designed for mobile robot localization. The Kalman filter (KF) is used as the main data fusion filter, where the state vector is composed of the position error, velocity error, yaw, and sampling time. The observation is provided of the difference between the LiDAR-derived and DR-derived distances measured from the corner feature points (CFPs) to the mobile robot. A real test experiment has been conducted to verify a good performance of the proposed method and show that it allows for a higher accuracy compared to the traditional LiDAR/DR integration.

Keywords: Light detection and ranging (LiDAR) · Dead Reckoning (DR) · Tightly integration · Uncertain sampling period

1 Introduction

Nowadays, mobile robots are widely exploited in indoor closed spaces Borenstein (2007). In view of the latter and as a basic issue for a robot to accomplish the task, the robot accurate localization has become a hot research topic Jiang (2015).

Many localization techniques were developed with time for indoor localization. For example, an effective weighted path length and support vector regression algorithm for radio frequency identification (RFID) is introduced in He (2018). An bluetooth-based accurate method is proposed for mobile robots and tested in Raghavan (2010). A WiFi-based solution is present to solve the localization problem for robots operating in unknown environments Benjamin (2015).

Y.-D. Zhang et al. (Eds.): ICMTEL 2020, LNICST 327, pp. 116–123, 2020.
https://doi.org/10.1007/978-3-030-51103-6_10

Although the received signal strength indication (RSSI)-based technology can also be used for indoor localization, it commonly provides an insufficient accuracy. In order to improve the localization accuracy, the ultra wide band (UWB) technology is developed for indoor needs Fan (2017). For instance, the UWB-based indoor robot localization system is designed Xu (2018). But, even though the UWB-based approach is able to improve the localization accuracy, it requires a pre-arranged additional equipment. In order to avoid an extra equipment, the beacon-free positioning approaches have been proposed. The famous example is an inertial navigation system (INS) Cai (2018). However, the INS-based schemes are not suitable for long-time operation due to induced time-drifts Wu (2019), Cao (2019). In this regard, the light detection and ranging (LiDAR) approach allows getting a higher positioning resolution in indoor environments Chang (2019), Akshay (2019) that is an obvious advantage.

In this paper, an tightly-coupled light detection and ranging (LiDAR)/dead reckoning (DR) navigation system is designed for mobile robot localization with uncertain sampling time. In this model, the Kalman filter (KF) is used as the main data fusion estimator. The state vector is composed of the position error, velocity error, yaw, and the sampling time. Observation is provided of the difference between the LiDAR-derived and DR-derived distances measured from the corner feature points (CFPs) to the mobile robot. A real test experiment is conducted to verify the performance and show that the system designed has a higher accuracy compared to the traditional LiDAR/DR integration schemes.

2 Tightly LiDAR/DR-Integrated Robot Localization Model

A block diagram of the tightly LiDAR/DR-integrated indoor mobile robot localization system designed is this paper is given in Fig. 1. In this scheme, the LiDAR provides measurements of the distance $\rho_i^L, i \in [1, n]$ between the mobile robot and the corner feature points (CFPs), where n is the numbers of the CFPs. The DR measures distances $\rho_i^D, i \in [1, n]$ between the mobile robot and the CFPs. The differences $\delta\rho^i = \rho_i^L - \rho_i^D, i \in [1, n]$, between the measured distances are used as measurements for the EKF. The vector output $\delta\mathbf{Po^D}$ of the EKF is used to compensate the vector drift $\mathbf{Po^D}$ in the DR.

Referring to Fig. 1, the state equation is written as

$$\underbrace{\begin{bmatrix} \delta Pe_t \\ \delta Pn_t \\ \delta V_t \\ \varphi_t \\ \Delta T_t \end{bmatrix}}_{\mathbf{x}_{t|t-1}} = \underbrace{\begin{bmatrix} \delta Pe_{t-1} + \Delta T_{t-1}\delta V_{t-1}\sin(\varphi_{t-1}) \\ \delta Pn_{t-1} + \Delta T_{t-1}\delta V_{tt-1}\cos(\varphi_{t-1}) \\ \delta V_{t-1} \\ \varphi_{t-1} \\ \Delta T_{t-1} \end{bmatrix}}_{a(\mathbf{x}_{t-1})} + \omega_{t-1}, \tag{1}$$

where t is the discrete time index, $(\delta Pe_{tt}, \delta Pn_{tt})$ is the DR-based position error, δV_{tt} is the DR-based velocity error, ϕ_{tt} is the mobile robot's yaw, the sampling time ΔT_t is considered as one of the states, and $\omega_t \sim \mathcal{N}(0, \mathbf{Q})$ is the system zero mean white Gaussian noise with the covariance $\mathbf{Q}$.

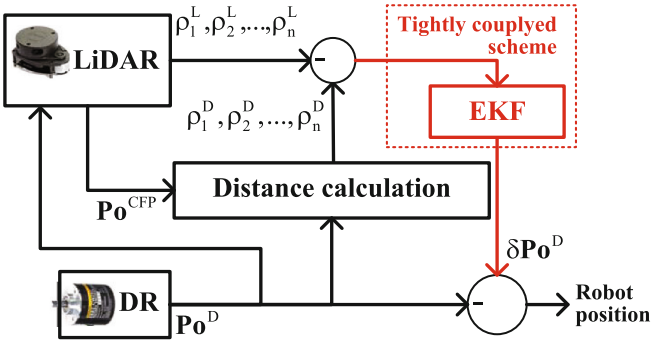

Fig. 1. Block diagram of the tightly LiDAR/DR-integrated indoor mobile robot localization system.

Based on the state equation, the distance ρ_i^D between the ith CFP and the mobile robot can be written as

$$\left(\rho_i^D\right)^2 = \left(Pe^D - Pe_i\right)^2 + \left(Pn^D - Pn_i\right)^2, i \in [1, n], \tag{2}$$

where (Pe_i, Pn_i) is the position of the ith CFP and $\left(Pe^D, Pn^D\right)$ is the DR-based position. A distance d_i^R between the ith CFP and the mobile robot can thus be specified by

$$\left(\rho_i^R\right)^2 = \left(Pe^R - Pe_i\right)^2 + \left(Pn^R - Pn_i\right)^2, i \in [1, n], \tag{3}$$

where $\left(Pe^R, Pn^R\right)$ is the real robot position. Because of $Pe^R = Pe^D - \delta Pe$ and $Pn^R = Pn^D - \delta Pn$, we have

$$\begin{aligned} &\left(\rho_i^D\right)^2 - \left(\rho_i^R\right)^2 \\ &= \left(Pe^D + Pe^R - 2Pe_i\right)\delta Pe + \left(Pn^D + Pn^R - 2Pn_i\right)\delta Pn. \end{aligned} \tag{4}$$

Moreover, ΔT_t is used as one the elements of the observation vector that, referring to the above, is written as

$$\underbrace{\begin{bmatrix} \delta\rho_{1,t} \\ \delta\rho_{2,t} \\ \vdots \\ \delta\rho_{g,t} \\ \Delta T_n \end{bmatrix}}_{\mathbf{y}_n} = \begin{bmatrix} \left(\rho_1^D\right)^2 - \left(\rho_1^L\right)^2 \\ \left(\rho_2^D\right)^2 - \left(\rho_2^L\right)^2 \\ \vdots \\ \left(\rho_g^D\right)^2 - \left(\rho_n^L\right)^2 \\ \Delta T_n \end{bmatrix}$$

$$= \underbrace{\begin{bmatrix} 2\left(Pe^D - Pe_1\right)\delta Pe + 2\left(Pn^D - Pn_1\right)\delta y - \left(\delta Pe^2 + \delta Pn^2\right) \\ 2\left(Pe^D - Pe_2\right)\delta Pe + 2\left(Pn^D - Pn_2\right)\delta y - \left(\delta Pe^2 + \delta Pn^2\right) \\ \vdots \\ 2\left(Pe^D - Pe_n\right)\delta Pe + 2\left(Pn^D - Pn_n\right)\delta y - \left(\delta Pe^2 + \delta Pn^2\right) \\ \Delta T_t \end{bmatrix}}_{h\left(\mathbf{x}_{t|t-1}\right)} + \nu_t \,, \tag{5}$$

where $\nu_t \sim N(0, \mathbf{R})$ is the zero mean white Gaussian measurement noise with the covariance $\mathbf{R}$.

3 Experiment

In this section, a real test measurement is conducted to verify the performance of the localization system designed. First, we will present the design of the LiDAR/DR integrated integration system. Then, the performance of the proposed method will be discussed.

Experimental investigations have been provided in the No. 1 teaching building of the University of Jinan, China. In this test, we employ one LiDAR, one DR, one mobile, and one computer. The LiDAR, DR, and a computer are maintained on a mobile robot. The LiDAR measures ranges $\rho_i^L, i \in [1, n]$, from the robot to the CFPs. The DR measures the velocity of the mobile robot and provides ranges $\rho_i^D, i \in [1, n]$ from the robot to the CFPs. A computer is used to collect the LiDAR- and DR-based ranges via the RS232. In this work, we set $\Delta T_t = 0.75\,\mathrm{s}$, which is also included to the observation vector listed in Eq. (5). Therefore, we suppose that ΔT_t is uncertain as it often is in digital systems and model it with

$$\Delta T_{tt} = 0.75 + \delta T, \tag{6}$$

where $\delta T \sim (0, 0.25)$ represents an uncertainty in the sampling time.

In Fig. 2 we sketch the reference path and the paths derived from DR and LiDAR. The reference trajectory and the ones derived by the LiDAR, LiDAR/DR tightly integration, and LiDAR/DR tightly integration with uncertain sampling period are shown in Fig. 3 and the position errors in east and north directions are sketched in Fig. 4. From these figures, one can deduce that the path estimated by the LiDAR/DR tightly integration has a large error due

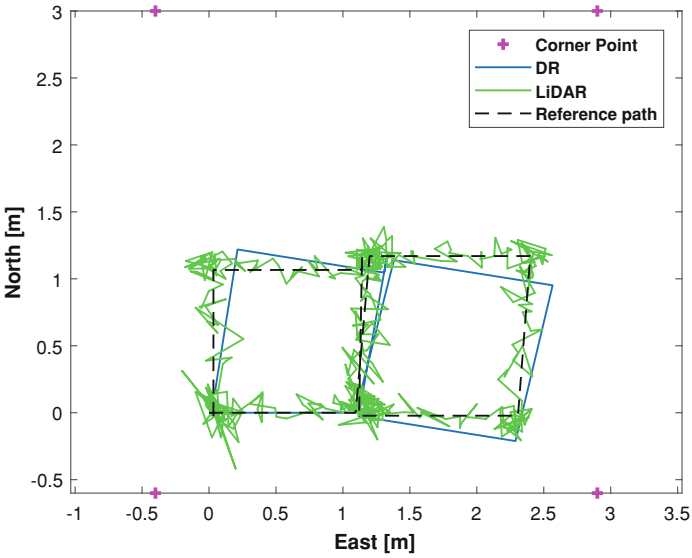

Fig. 2. The reference path and the paths derived from the DR and LiDAR.

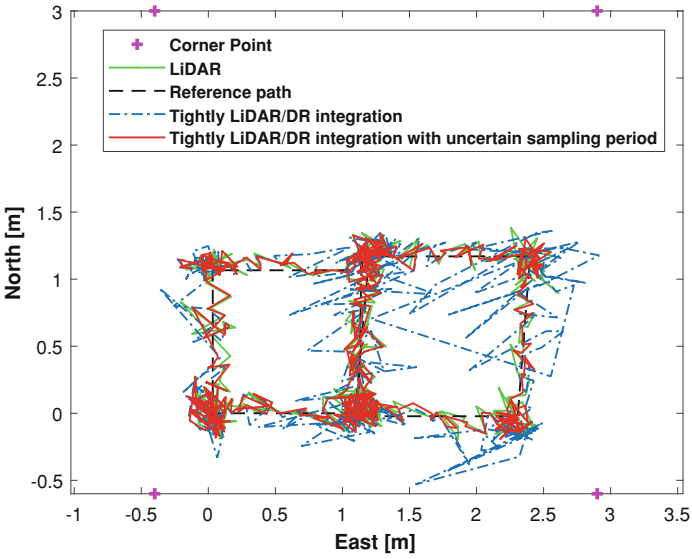

Fig. 3. The reference trajectory and ones derived by the LiDAR, LiDAR/DR tightly integration, and LiDAR/DR tightly integration schemes with uncertain sampling time.

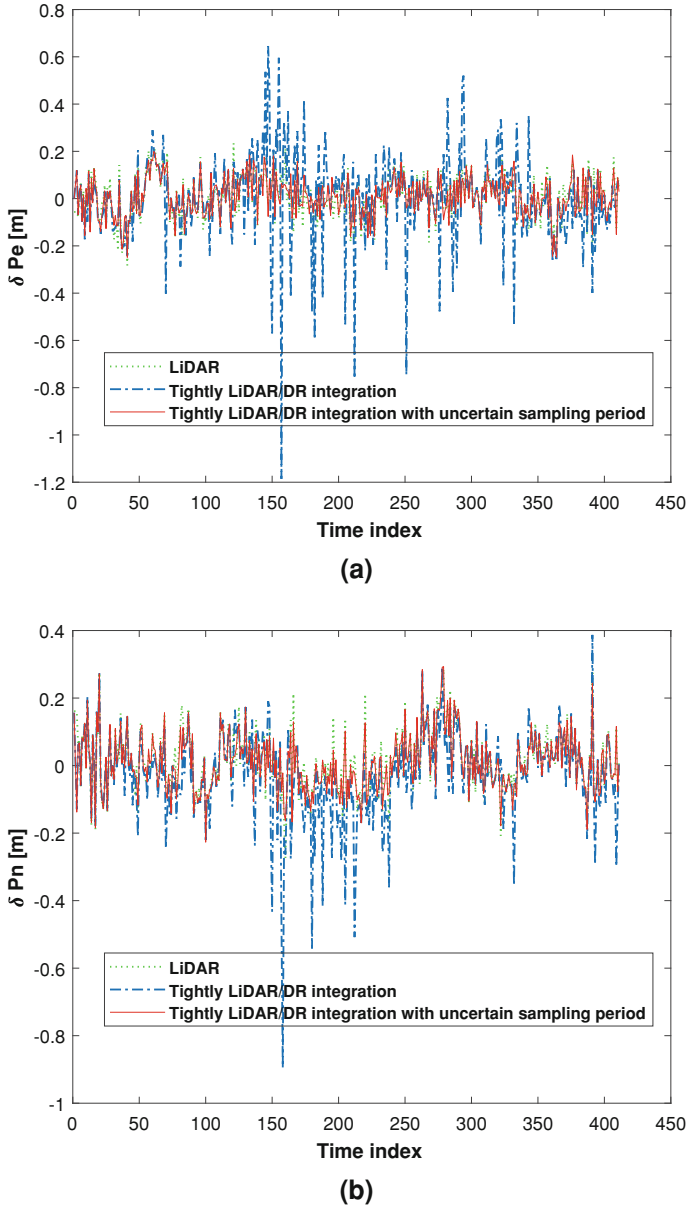

Fig. 4. Position errors estimated by the LiDAR, LiDAR/DR integration, and LiDAR/DR integration with uncertain sampling time: (a) east direction (b) north direction.

to the uncertain sampling time. Compared to the traditional tightly integration, the proposed LiDAR/DR tightly integration with uncertain sampling time has a stable performance. The root mean square error (RMSE) produced by the DR and LiDAR in the east and north directions are listed in Table 1. For the uncertain sampling time, the RMSEs are listed in Table 2.

Table 1. RMSE produced by DR and LiDAR

Method	RMSE (m)	
	East	North
DR	0.1186	0.1128
LiDAR	**0.0917**	**0.0896**

Table 2. RMSE produced nu LiDAR, LiDAR/DR, and LiDAR/DR with uncertain sampling time

Method	RMSE (m)	
	East	North
LiDAR	0.0917	0.0896
LiDAR/DR	0.1793	0.1290
LiDAR/DR with uncertain sampling time	**0.0832**	**0.0850**

Observing these tables, one concludes that the proposed localization scheme has the highest accuracy.

4 Conclusion

The tightly LiDAR/DR-integrated system with uncertain sampling time has been designed for indoor robot localization. The position error, velocity error, yaw, and uncertain sampling time were selected as components of the state vector of the tightly integrated model. The proposed model employs the difference between the LiDAR- and DR-derived distances measured from the CFPs to the mobile robot and combined in the observation vector. Real test measurements conducted in No. 1 teaching building of the University of Jinan, China, have confirmed a highest accuracy of the solution proposed among other available schemes, including the traditional LiDAR/DR integration. An overall conclusion that can be made is that the performance of the proposed tightly model is better than that demonstrated by traditional methods.

Acknowledgment. This work was supported by the Shandong Key R&D Program under Grants 2019GGXI04026 and 2019GNC106093.

References

Jiang, W., Li, Y., Rizos, C.: Precise indoor positioning and attitude determination using terrestrial ranging signals. J. Navig. **68**(2), 274–290 (2015)

He, X., Wu, M., Li, P., et al.: An RFID indoor positioning algorithm based on support vector regression. Sensors **18**(5), 1504 (2018)

Raghavan, A.N., Ananthapadmanaban, H., Sivamurugan, M.S., et al.: Accurate mobile robot localization in indoor environments using bluetooth. In: IEEE International Conference on Robotics and Automation (2010)

Benjamin, B., Erinc, G., Carpin, S.: Real-time WiFi localization of heterogeneous robot teams using an online random forest. Auton. Robots **39**(2), 155–167 (2015). https://doi.org/10.1007/s10514-015-9432-5

Fan, Q., Sun, B., Sun, Y., et al.: Data fusion for indoor mobile robot positioning based on tightly coupled INS/UWB. J. Navig. **70**(5), 1079–1097 (2017)

Xu, Y., Shmaliy, Y.S., Ahn, C.K., et al.: Robust and accurate UWB-based indoor robot localisation using integrated EKF/EFIR filtering. IET Radar Sonar Navig. **12**(7), 750–756 (2018)

Cai, X., Hsu, H., Chai, H., et al.: Multi-antenna GNSS and INS integrated position and attitude determination without base station for land vehicles. J. Navig. **72**(2), 342–358 (2019)

Cao, H., Zhang, Y., Han, Z., et al.: Pole-zero-temperature compensation circuit design and experiment for dual-mass MEMS gyroscope bandwidth expansion. IEEE/ASME Trans. Mechatron. **24**(2), 677–688 (2019)

Wu, Z., Wang, W.: INS/magnetometer integrated positioning based on neural network for bridging long-time GPS outages. GPS Solut. **23**(3), 1–11 (2019). https://doi.org/10.1007/s10291-019-0877-4

Akshay, S., Gao, G.X.: Adaptive covariance estimation of LiDAR-based positioning errors for UAVs. Navig.-J. Inst. Navig. **66**(2), 463–476 (2019)

Chang, L., Niu, X., Liu, T., et al.: GNSS/INS/LiDAR-SLAM integrated navigation system based on graph optimization. Remote Sens. **11**(9), 1009 (2019)

Borenstein, L., Johann, O.: Non-GPS navigation for security personnel and first responders. J. Navig. **60**(3), 391–407 (2007)

Xu, Y., Shmaliy, Y.S., Li, Y., Chen, X., Guo, H.: Indoor INS/LiDAR-based robot localization with improved robustness using cascaded FIR filter. IEEE Access **7**(1), 34189–34197 (2019)